

Multiple transitions in vacuum dark energy and H_0 tension

HOSSEIN MOSHAFI,¹ HASSAN FIROUZJAH, ¹ AND ALIREZA TALEBIAN¹¹*School of Astronomy, Institute for Research in Fundamental Sciences (IPM)
P. O. Box 19395-5531, Tehran, Iran*

(Dated: August 12, 2022)

ABSTRACT

We study the effects of multiple transitions in the vacuum dark energy density on the H_0 tension problem. We consider a phenomenological model in which the vacuum energy density undergoes multiple transitions in the early as well as the late universe and compare the model's predictions using the three sets of data from CMB+BAO+SN. The transient dark energy can be either positive (dS-like) or negative (AdS-like). We conclude that a transient late-time AdS-type vacuum energy typically yields the higher value of H_0 which can alleviate the H_0 tension. In addition, to obtain a value of H_0 comparable to the value obtained from the local cosmological measurements the spectral index n_s moves towards its Harrison-Zel'dovich scale invariant value.

1. INTRODUCTION

The disagreement between the independent measurements of the Hubble constant, based on the early universe with the Λ CDM model and that measured by direct observations of the local universe without assuming the Λ CDM model, is dubbed as the Hubble tension (Di Valentino et al. 2021a; Perivolaropoulos & Skara 2021; Verde et al. 2019; Riess 2019; Di Valentino et al. 2021b; Schöneberg et al. 2021; Dainotti et al. 2021, 2022). More precisely, the reported value of the Hubble parameter from the Planck satellite is $H_0 = 67.4 \pm 0.5$ Km/s/Mpc (Aghanim et al. 2020b) while the latest SH0ES Team (Riess et al. 2021) has reported $H_0 = 73.30 \pm 1.04$ Km/s/Mpc. This tension is an important open problem in cosmology. Ignoring the possible systematics origin of the tension (Freedman et al. 2019; Efstathiou 2020; Mortsell et al. 2021), it is natural to expect that either a modification to the cosmological model is required or there is a new physics behind the tension (Mortsell & Dhawan 2018; Guo et al. 2019; Vagnozzi 2020; Di Valentino et al. 2016; Knox & Millea 2020; Schöneberg et al. 2021).

Qualitatively speaking, there are two classes of models attempting to resolve the Hubble tension by introducing new physics. The first class of models are based on the modifications in dark components at late times (i.e., lower redshifts),

e.g., by introducing a dynamical dark energy that alter the Hubble expansion. In the second class of models, the new physics aims to reduce the sound horizon by $\sim 7\%$ (Bernal et al. 2016; Lemos et al. 2019; Knox & Millea 2020) while keeping the Baryon Acoustic Oscillation (BAO) and the uncalibrated SNeIa data to be consistent with Planck measurements. The locations of the acoustic peaks in the CMB observations is one of the most precisely measured quantity in cosmology. With an accuracy of 0.03% the Planck satellite (Aghanim et al. 2020b) has determined the angular size of the sound horizon at recombination, $\theta_* \equiv r_*/D_*$, in which the sound horizon r_* is the comoving distance a sound wave could travel from the beginning of the universe to the time of recombination, and D_* is the comoving integrated distance from now to the epoch of recombination. D_* depends only on two parameters Ω_m (the fractional matter energy density today) and the present value of Hubble expansion rate, H_0 . Thus, given r_* and an estimation of Ω_m , one can infer H_0 from the measurement of θ_* . Using the Planck best fit values of Ω_m and r_* in the context of the Λ CDM model (Aghanim et al. 2020b), H_0 is found to be significantly lower than the more direct local measurements. If the value of the Hubble constant from SH0ES is considered, it would yield a much larger value of θ_* unless either r_* and/or D_* were modified to preserve the observed CMB acoustic peak positions.

Pre-recombination early dark energy (EDE) (Karwal & Kamionkowski 2016; Poulin et al. 2019; Kaloper 2019; Agrawal et al. 2019; Lin et al. 2019; Smith et al. 2020; Niedermann & Sloth 2021; Sakstein & Trodden 2020; Ye & Piao 2020a; Gogoi et al. 2021; Braglia et al. 2020; Lin et al. 2020;

moshafi@ipm.ir

firouz@ipm.ir

talebian@ipm.ir

Seto & Toda 2021; Nojiri et al. 2021; Karwal et al. 2022) is one of the best-studied scenario as a solution to the Hubble tension. In this scenario, a dark energy-like component is introduced. The energy injection before recombination boosts the Hubble expansion rate (by reducing the sound horizon). The EDE then decays rapidly in order not to spoil other observations. Various scenarios have been proposed for both the early energy injection (Poulin et al. 2019; Kaloper 2019; Agrawal et al. 2019; Lin et al. 2019; Smith et al. 2020; Niedermann & Sloth 2021; Sakstein & Trodden 2020; Ye & Piao 2020a; Gogoi et al. 2021; Braglia et al. 2020; Lin et al. 2020; Seto & Toda 2021; Nojiri et al. 2021; Karwal et al. 2022; Zumalacarregui 2020; Ballesteros et al. 2020; Braglia et al. 2021) and the decaying processes (Poulin et al. 2019; Smith et al. 2020; Ye & Piao 2020a).

EDE models have important effects on primordial scalar perturbations and on Large-Scale Structure (LSS) physics. It has been found that the EDE models require a re-interpretation of the available data, resulting in higher values of n_s , all the way up to a scale-invariant Harrison-Zeldovich spectrum of primordial scalar perturbation, i.e. $n_s = 1$ (Di Valentino et al. 2018; Ye et al. 2021a; Jiang & Piao 2022). The second effect of EDE models appears when one considers the galaxy clustering data (Krishnan et al. 2020; Hill et al. 2020; Ivanov et al. 2020; D’Amico et al. 2021). Although a large EDE fractions f_{EDE} are not ruled out by these datasets (Murgia et al. 2021; Smith et al. 2021; Herold et al. 2022; Gómez-Valent 2022), increasing f_{EDE} will increase the clustering amplitude σ_8 and the related value of S_8 (Di Valentino & Bridle 2018; Nunes & Vagnozzi 2021). In other word, the models with a large fractions f_{EDE} worsen the well-known “ S_8 discrepancy”. Most of EDE models proposed as a solution to the Hubble tension leads to an increase of clustering amplitude (S_8) that worsen the fit to galaxy clustering data. Ref. (Reeves et al. 2022) argued that freeing the total neutrino mass M_ν can suppress small-scale power and then improve EDE’s fit to galaxy clustering data.

Currently, the most precise large-scale CMB observation is Planck data, which alone seems not to favour axion-like EDE models (Hill et al. 2020). However, the TT power spectrum of Planck data, especially in small scales, needs more considerations. Some inconsistencies between the $\ell_{\text{TT}} < 1000$ and $\ell_{\text{TT}} > 1000$ part of Planck’s TT power spectrum have been reported in Refs. (Addison et al. 2016; Aghanim et al. 2017). Moreover, the amplitude of CMB gravitational lensing in Planck data is not consistent with what we expect in Λ CDM model. The smoothing effect of gravitational lensing on acoustic peaks of the CMB power spectrum exceeds that expected in Λ CDM model (Addison et al. 2016; Motloch & Hu 2020). However, small scale ground-based CMB observations such as ACT and SPT, providing precise measurements on small scale power spectrum, have not found

this over-smoothing effect (Henning et al. 2018; Aiola et al. 2020; Dutcher et al. 2021). Recently, combined analysis of Planck ($\ell_{\text{TT}} \lesssim 1000$) with ACT and SPT data for EDE models has also been performed, such as CMB+SPTpol (Chudaykin et al. 2020, 2021; Jiang & Piao 2021), CMB+ACT DR4 (Hill et al. 2021; Poulin et al. 2021) and CMB+ACT DR4+SPT-3G (La Posta et al. 2021; Smith et al. 2022; Jiang & Piao 2022). Also for CMB+LSS data see (Hill et al. 2020; Ivanov et al. 2020; D’Amico et al. 2021; Ye et al. 2021b).

In this paper, we study a scenario with multiple transient phases of dark energy, both before and after the surface of last scattering, yielding to a higher value of the current Hubble expansion rate compared to what is inferred from the Λ CDM model. This is a phenomenological model motivated from (Firouzjahi 2022b) where the quantum vacuum zero point energy in connection to cosmological constant problem and the origin of dark energy were studied. Alternatively, the current setup may be viewed as an independent phenomenological mechanism with some similarities to the EDE proposal. For other works involving phase transitions in dark energy and their impacts on H_0 tension see also (Banihashemi et al. 2020; Farhang & Khosravi 2021; Khosravi & Farhang 2022; Moshafi et al. 2021).

2. THE MODEL

We consider the model consisting of some new energy density source ρ_x arising from the quantum zero point energy of the fields with the mass m . Depending on the type of the quantum field (boson or fermion) and the energy scale of interest ρ_x can be either positive (dS-like) or negative (AdS-like) (Martin 2012; Firouzjahi 2022b,a). For the sake of simplicity, here first we consider the case of a single quantum field while the procedure for the multiple field is straightforward thanks to our simplifying assumption that the vacuum energies of the free fields do not exchange with each other.

Associated to the energy density ρ_x , we can define a horizon radius, denoted by H_x^{-1} , in which $3M_P^2 H_x^2 = |\rho_x|$ in which M_P is the reduced Planck mass. Let us also denote H as the Hubble rate of the observable FLRW universe with $3M_P^2 H^2 = \rho$ in which ρ is the total energy density. Depending on the mass scale m , the contribution of ρ_x can be viewed as a source of dark energy in ρ . At the early stage in cosmic expansion history the zero point energy of the field appears as a small constant term in ρ . More specifically, $\rho_x = cm^4$ with c is a constant. As illustrated in left panel of Fig. 1 in this regime $H^{-1} \ll H_x^{-1}$ so the FLRW horizon (at that time) is within one patch of the vacuum energy. As time proceeds and ρ decreases further, we can indicate a specific scale factor a_c (or redshift z_c) when $\rho(a_c) \sim \rho_x \sim m^4$. At this stage in cosmic epoch $H_x^{-1} \sim H^{-1}$, as in the middle panel of Fig. 1, and ρ_x can be relevant as the source of dark energy at that time. After this phase, ρ falls off rapidly

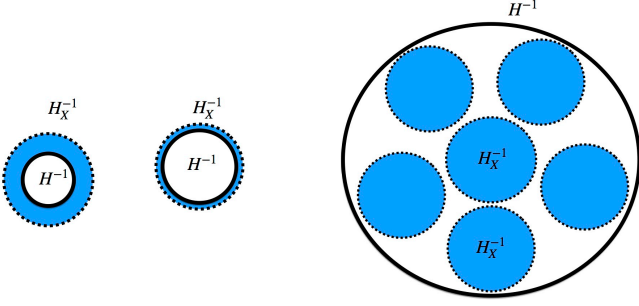


Figure 1. A schematic view of the evolution of dark energy ρ_x compared to total energy density ρ . Left: at early times $\rho_x \ll \rho$ and $H_x^{-1} \gg H^{-1}$ so the FLRW horizon is within one patch of dS horizon associated to dark energy. Middle: around the time of transition $\rho_x \sim \rho$ and $H_x^{-1} \sim H^{-1}$. This is the time when the effects of dark energy become important. Right: long after transition, many patches of dS horizon associated to ρ_x enter the FLRW horizon and the effects of ρ_x are represented by a phenomenological fluid with the equation of state w .

and very soon we have $H^{-1} \gg H_x^{-1}$, as illustrated in right panel of Fig. 1. It is argued in (Firouzjahi 2022b) that as many patches of vacuum horizon with the size H_x^{-1} enters the FLRW horizon the patches of zero point energy develops inhomogeneities $\frac{\delta \rho_x}{\rho_x} > 1$. The subsequent evolution of ρ_x on sub Hubble scale is left as an open problem in (Firouzjahi 2022b). The time of the transition in dark energy is determined by the mass of the quantum field, happening at the temperature $T_c \sim m$. For example, for the simplest model in Standard Model (SM) with three massive neutrinos, we can have three transitions in dark energy in which the first transition may happen shortly after the time of CMB decoupling while the other two transitions may happen much later in cosmic expansion history. In addition, the current stage of dark energy may be associated with the zero point energy of the lightest neutrino field with the mass $m_\nu \sim 10^{-2} \text{eV}$.

Motivated by the above discussions, we picture the effects of ρ_x after the time when $a > a_c$ by a phenomenological dark fluid with the equation of state w . In this phenomenological view, ρ_x is constant at early universe ($a \ll a_c$) and dilutes as $a^{-3(1+w)}$ at late time ($a \gg a_c$). The requirement that the energy density of the dark fluid does not overclose the universe too early, we expect that ρ_x to fall off faster than radiation, so we impose $\frac{1}{3} < w \leq 1$. In addition, we keep the position of the transition to be free. In practice, motivated by EDE proposal, we take the position of the first step (first transition) to be after the time of matter radiation equality and before the CMB decoupling around the redshift $z_c \sim 2000 - 3000$ while the follow up transitions can happen

much later in cosmic expansion history. Within the model of (Firouzjahi 2022b) this corresponds to a field with the mass $m \sim \text{eV}$. As a field with this mass is not within the spectrum of SM, one needs a new physics beyond SM. For example, this may come from an eV-scale sterile neutrino e.g. from short-baseline anomalies but this is tightly constrained, see for example (Hagstotz et al. 2021).

The simplest model satisfying our requirements may be realized by the following ansatz,

$$\rho_x(a) \propto \left[1 + \left(\frac{a}{a_c} \right)^{3(1+w)} \right]^{-1}. \quad (1)$$

At early stages, $a \ll a_c$ in which a_c is the transition scale factor, $\rho_x(a)$ is nearly constant but small while long after the transition it falls off like $a^{-3(1+w)}$. However, to control the sharpness of dark energy transition we introduce a transfer function $\mathcal{T}(b, a - a_c)$ in which b is a positive constant parameter measuring the sharpness of transition. In our analysis we consider the following transfer function

$$\mathcal{T}(b, a - a_c) = \frac{1}{2} \left[1 + \tanh(b(a - a_c)) \right]. \quad (2)$$

For $b|a - a_c| \gg 1$, the transfer function \mathcal{T} behaves like the Heaviside function $\Theta(a - a_c)$ indicating a sharp transition while for $b|a - a_c| \ll 1$, \mathcal{T} describes a mild transition.

With the inclusion of the above transfer function, Eq. (1) is modified as

$$\rho_x(a) = \rho_{x,c} \left[\mathcal{T}(b, a_c - a) + \mathcal{T}(b, a - a_c) \left(\frac{a}{a_c} \right)^{3(1+w)} \right]^{-1}, \quad (3)$$

where $\rho_{x,c} = \rho_x(a = a_c)$. At the transition scale factor a_c , we introduce the fraction of dark energy density f_x associated to the field (or dark fluid) as

$$f_x \equiv \frac{\rho_{x,c}}{\rho(a_c)}, \quad (4)$$

where $\rho(a)$ is the total energy density in the Friedmann equation, $3M_P^2 H^2 = \rho(a)$, and is given by

$$\rho(a) = \rho_m a^{-3} + \rho_r a^{-4} + \rho_\Lambda + \rho_x(a), \quad (5)$$

in which ρ_m, ρ_r and ρ_Λ respectively are the present value ($a = 1$) of matter, radiation and the dark energy density of the universe. At the transition scale a_c we find

$$\rho(a_c) = \frac{\rho_m a_c^{-3} + \rho_r a_c^{-4} + \rho_\Lambda}{1 - f_x}, \quad (6)$$

and then

$$\rho_{x,c} = \frac{f_x}{1 - f_x} (\rho_m a_c^{-3} + \rho_r a_c^{-4} + \rho_\Lambda). \quad (7)$$

Note that for dS-like (AdS-like) dark energy $f_x > 0$ ($f_x < 0$).

Plugging the above value in Eq. (5), the total energy density of our model is given by

$$\rho(a) = \rho_m a^{-3} + \rho_r a^{-4} + \rho_\Lambda + \frac{\frac{f_x}{1-f_x}(\rho_m a_c^{-3} + \rho_r a_c^{-4} + \rho_\Lambda)}{\mathcal{T}(b, a_c - a) + \mathcal{T}(b, a - a_c) \left(\frac{a}{a_c}\right)^{3(1+w)}}. \quad (8)$$

The fraction of the current energy density Ω_i for each component can easily be calculated. At present, $3M_P^2 H_0^2 = \rho_0$, we have

$$\rho_0 = \rho_m + \rho_r + \rho_\Lambda + \rho_{x,0}, \quad (9)$$

in which $\rho_{x,0} = \rho_x(a=1)$. Correspondingly, for each component in cosmic fluid we have

$$\Omega_m = \frac{\rho_m}{\rho_0}, \quad \Omega_r = \frac{\rho_r}{\rho_0}, \quad \Omega_\Lambda = \frac{\rho_\Lambda}{\rho_0}, \quad \Omega_x = \frac{\rho_{x,0}}{\rho_0}. \quad (10)$$

As a rough estimation of Ω_x , using the simple form of ρ_x from Eq. (1), the fraction of dark energy density is obtained to be

$$\Omega_x = \frac{2f_x}{1-f_x} \frac{a_c^{3w}}{1+a_c^{3w}} [\Omega_m + \Omega_r a_c^{-1} + \Omega_\Lambda a_c^3]. \quad (11)$$

For the early time when $a_c \ll 1$ we approximately obtain,

$$\Omega_x \simeq \frac{2f_x}{1-f_x} a_c^{3w} [\Omega_m + \Omega_r a_c^{-1}]. \quad (12)$$

If we further assume that $a_c \ll a_{\text{eq}}$, i.e. the transition happens after the matter radiation equality, then the above relation simplifies further to

$$\Omega_x \simeq \frac{2f_x}{1-f_x} a_c^{3w} \Omega_m. \quad (13)$$

Note that the parameter Ω_x is what defined in (Karwal & Kamionkowski 2016) as Ω_{ee} . For $a_c \lesssim 10^{-3}$ and $f \sim 0.1$, with $w = 1$, we typically have $\Omega_x \sim 10^{-10}$ or so. For $a_c \sim 10^{-1}$ and $w = 1$, we obtain $\Omega_x \sim 10^{-5}$. So in general for $w > \frac{1}{3}$, Ω_x is smaller than $\Omega_r \sim 10^{-4}$.

For the N -field configuration, yielding to N transitions in dark energy at $a_{c,i}$ with $i = 1, 2, \dots, N$, one can extend (8) to the following form

$$\rho(a) = \rho_{m,0} a^{-3} + \rho_{r,0} a^{-4} + \rho_\Lambda + \sum_{i=1}^N \frac{\frac{f_i}{1-f_i}(\rho_m a_{c,i}^{-3} + \rho_r a_{c,i}^{-4} + \rho_\Lambda)}{\mathcal{T}(b_i, a_{c,i} - a) + \mathcal{T}(b_i, a - a_{c,i}) \left(\frac{a}{a_{c,i}}\right)^{3(1+w_i)}} \quad (14)$$

In the following analysis, we also parameterize b_i as

$$b_i \equiv \frac{10^{n_i}}{a_{c,i}}. \quad (15)$$

For a sharp phase transition in dark energy with $b_i a_{c,i} \gg 1$, we have $n_i > 0$ while for a mild transition $n_i < 0$.

In summary, the new parameters of the model are $\{f_i, a_{c,i}, n_i, w_i\}$ for each component $i = 1, 2, \dots, N$ of dark fluid. f_i measures the fraction of dark energy at the time of transition $a_{c,i}$ (or $z_{c,i}$), n_i measures the sharpness of the transition and w_i represents the equation of state of the dark fluid after the transition $a(t) > a_{c,i}$.

Our model has some similarities to EDE setup in which we consider an early stage of dark energy. However, we include the new parameter n_i to control how sharp the transition has happened. Moreover, with our theoretical motivations in mind, we allow for multiple transitions in dark energy during the Universe evolution, $N \geq 1$. In addition, the contributions of the subsequent dark fluids ($1 < i \leq N$) can be either dS ($f_i > 0$) or AdS ($f_i < 0$). For earlier works concerning AdS vacua and H_0 tension or AdS-EDE see Calderón et al. (2021); Ruchika et al. (2020); Dutta et al. (2020); Visinelli et al. (2019); Akarsu et al. (2020, 2021); Ye & Piao (2020a); Jiang & Piao (2021); Ye & Piao (2020b); Sen et al. (2021).

There is an important comment in order. In the current analysis of studying the effects of multiple transitions in dark energy, we concentrate on the background evolution and do not study perturbations. In our setup the physical mechanism behind the dark energy transitions and the transfer of energy to thermal bath are already complicated phenomena at the background level and a full treatment of perturbations analysis is beyond the scope of the current analysis. While studying the background dynamics can shed some light on the H_0 tension problem, but it is not fully consistent. This is an important limitation in our current analysis which should be improved in future studies considering the full dynamics of the background and the perturbations.

3. OBSERVATIONAL DATA AND STATISTICAL METHODOLOGY

In this section, we begin with a brief description of the main cosmological data sets used in this work. In all of our analysis we consider a combination of three types of data: ‘‘CMB+BAO+SN’’.

1. **CMB:** We use the latest most precise large-scale cosmic microwave background (CMB) temperature and polarization angular power spectra from the final release of ‘‘Planck 2018’’ `plikTTTEEE+lowl+lowE` (Aghanim et al. 2020b,c,a). We use full power spectrum and don't split into high- ℓ and low- ℓ parts. We

mention all of Planck data (including temperature and polarization) by “CMB”.

2. **BAO:** We also take into account the various measurements of the Baryon Acoustic Oscillations (BAO) from different galaxy surveys [Aghanim et al. \(2020b\)](#), i.e. 6dFGS [Beutler et al. \(2011\)](#), SDSS-MGS [Ross et al. \(2015\)](#), and BOSS DR12 [Alam et al. \(2017\)](#).
3. **SN:** We include the measurements of the 1048 Supernovae Type Ia luminosity distance in the red-shift interval $z \in [0.01, 2.3]$, from the Pantheon sample ([Scolnic et al. 2018](#)). We show this catalog of SuperNovae by “SN”.

To analyze the data and extract the constraints on the cosmological parameters, we have modified the well known cosmological MCMC package `cosmoMC` ([Lewis & Bridle 2002](#); [Lewis 2013](#)), which is publicly available¹. This package is equipped with a convergence diagnostic based on the Gelman and Rubin statistic ([Gelman & Rubin 1992](#)), assuming $R - 1 < 0.1$, and implements an efficient sampling of the posterior distribution using the fast/slow parameter decorrelations ([Lewis 2013](#)).

Parameter space for Λ CDM model is:

$$\mathcal{P}_0 \equiv \left\{ \Omega_b h^2, \Omega_c h^2, 100\theta_{\text{MC}}, \tau, n_s, \ln[10^{10} A_s] \right\}, \quad (16)$$

where τ is the reionization optical depth, n_s is the scalar spectral index, A_s is the amplitude of the scalar primordial power spectrum, and the θ_{MC} parameter is an approximation of θ_* .

The set of free parameters describing the One-Step class of models (i.e. one transition in dark energy, $N = 1$) is given by

$$\mathcal{P}_1 \equiv \left\{ a_1, f_1, w_1, n_1, \Omega_b h^2, \Omega_c h^2, 100\theta_{\text{MC}}, \tau, n_s, \ln[10^{10} A_s] \right\}. \quad (17)$$

Correspondingly, the parameter space of Two-Step class of models ($N = 2$) is given by

$$\mathcal{P}_2 \equiv \left\{ a_1, f_1, w_1, n_1; a_2, f_2, w_2, n_2; \Omega_b h^2, \Omega_c h^2, 100\theta_{\text{MC}}, \tau, n_s, \ln[10^{10} A_s] \right\}. \quad (18)$$

Subsequently, the set of free parameters representing parameter space for Three-Step class of models ($N = 3$) is given by

$$\mathcal{P}_3 \equiv \left\{ a_1, f_1, w_1, n_1; a_2, f_2, w_2, n_2; a_3, f_3, w_3, n_3; \Omega_b h^2, \Omega_c h^2, 100\theta_{\text{MC}}, \tau, n_s, \ln[10^{10} A_s] \right\}. \quad (19)$$

¹ <http://cosmologist.info/cosmomc>

4. RESULTS

For testing our proposal we consider three main classes of models: **One-Step**, **Two-Step** and **Three-Step** models which in each class we assume there is a transition in dark energy density. For simplicity we begin with One-Step models and continue to Two-Step and Three-Step class of models. We will test the effects of step-position $z_{c,i}$, strength of fraction of total energy density f_i and also the effects of having dS ($f_i > 0$) or AdS ($f_i < 0$) phases of evolution in the following subsections.

4.1. One-Step models

4.1.1. Effects of step position

In this subsection we consider One-Step models that are different in the position $z_{c,1}$ when the transition in dark energy takes place. In Table. 1 we see our considered priors for this class of models. When we let the step position “ $z_{c,1}$ ” and the fraction of energy density “ f_1 ” both to be free parameters we had some computational problems. Therefore, we decided to test our hypothesis by assuming these two parameters to be fixed in each run but to have different values in each run. So, in this and the rest of our analysis we assume the step positions and the fraction of total energy density to be fixed parameters but to have different fixed values in each analysis.

In Table. 2 we summarize observational constraints of this class of models by considering Λ CDM as an anchor. We point out that in all of the analysis of models we use a combination of three types of data i.e. “CMB+BAO+SN”.

Looking at Table. 2 it is obvious that Model 3 shows the least tension with the SH0ES results. In this model we assume the transition in dark energy occurs at $z \simeq 2500$ which is deeply before the surface of last scattering and after the time of matter-radiation equality. Our conclusion for One-Step models is that an early phase of dark energy with $f_1 > 0$, as in EDE scenario, can reconcile the H_0 tension. On the other hand, One-Step models with transition happening after the surface of last scattering are not promising for this purpose.

The effects of considering early step in density evolution are shown in Fig. 2. In this figure we see the likelihoods of different One-Step models with different step-positions. Also, contour plots for parameters H_0 and Ω_m can be seen in Fig. 3.

4.1.2. Effects of the strength of the fraction of dark energy density

In this section we look at the effects of the fraction of dark energy density in One-Step class of model. We summarize our consideration for priors in this analysis in Table. 3. According to our past analysis we choose a fixed step position at $a_{c,1} = 0.0004$ ($1 + z_{c,1} = 2500$) and also fixed the fraction of dark energy density f_1 but with different values in each

Parameter	Priors Model 1	Priors Model 2	Priors Model 3
$1 + z_{c,1}$	25	250	2500
f_1	0.20	0.20	0.20
w_1	[0.5, 1]	[0.5, 1]	[0.5, 1]
n_1	[-1, 1.5]	[-1, 1.5]	[-1, 1.5]

Table 1. Priors for **One-Step** models for different step positions. Note that we take the fraction of dark energy density f_1 for all cases to be the same while let w_1 and n_1 to vary. The redshift of the step position is denoted by $1 + z_{c,1}$ and test the model in three different step positions: before recombination, after recombination and late-time era.

Parameter	Best-fit Λ CDM	Best-fit Model 1	Best-fit Model 2	Best-fit Model 3
n_1	---	> 0.945	> 1.18	> 1.46
w_1	---	> 0.880	> 0.923	0.808 ± 0.060
Ω_m	0.3092 ± 0.0070	0.3107 ± 0.0073	0.3040 ± 0.0068	0.2838 ± 0.0085
H_0	67.70 ± 0.52	66.43 ± 0.54	67.80 ± 0.52	$71.83^{+0.59}_{-0.67}$
S_8	0.819 ± 0.014	0.793 ± 0.014	$0.803^{+0.013}_{-0.015}$	0.890 ± 0.018
$10^9 A_s$	2.091 ± 0.027	$2.069^{+0.025}_{-0.028}$	2.086 ± 0.027	2.052 ± 0.029
n_s	0.9668 ± 0.0042	0.9795 ± 0.0044	0.9681 ± 0.0042	0.9932 ± 0.0044
τ	0.0541 ± 0.0059	0.0544 ± 0.0058	0.0551 ± 0.0059	0.0425 ± 0.0065

Table 2. %68 limits for parameters of **One-Step** models with different step positions (cf. table 1) in comparison with Λ CDM model based on CMB+BAO+SN data.

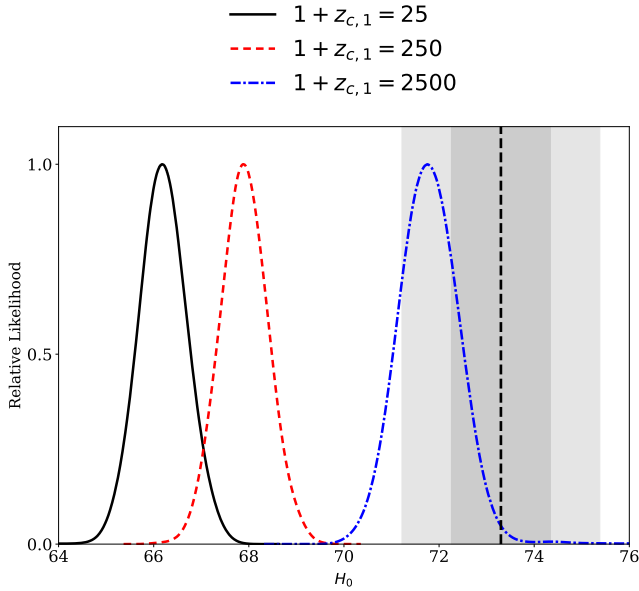


Figure 2. One-dimensional likelihoods for **One-Step** models for H_0 based on “CMB+BAO+SN” data. Note that the shaded area shows measurement of H_0 done by SH0ES team and its 1σ error (Riess et al. 2021).

analysis. Both of w_1 and n_1 are free parameters in all of our analysis.

The conclusion is that the higher is the value of f_1 , the larger is the prediction for H_0 . As we see in Table. 4

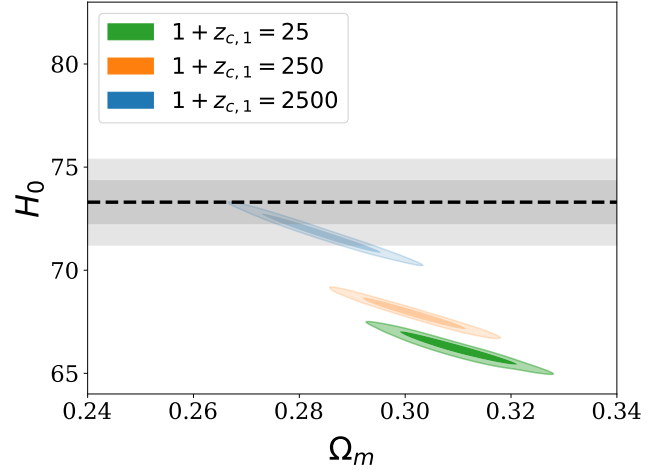


Figure 3. Contour plots for **One-Step** models for H_0 vs. Ω_m based on CMB+BAO+SN data. Note that the shaded area shows measurement of H_0 done by SH0ES team and its 1σ error (Riess et al. 2021).

Model 5 which has higher value of fraction of energy density ($f_1 = 0.25$) shows more consistency with the value of H_0 from SH0ES measurements. As we reported in Table. 13 the Gaussian tension in H_0 for model 5 is just 0.47σ .

In Fig. 4 we present the likelihood probabilities for One-Step class of models with different values for f_1 . Also, the two-dimensional contour plots for parameters H_0 vs. Ω_m are shown in Fig. 5. In both figures the shaded area are 1σ and

Parameter	Priors Model 4	Priors Model 3	Priors Model 5
$1 + z_{c,1}$	2500	2500	2500
f_1	0.15	0.20	0.25
w_1	[0.5, 1]	[0.5, 1]	[0.5, 1]
n_1	[-1, 1.5]	[-1, 1.5]	[-1, 1.5]

Table 3. Priors for **One-Step** models for different f_1 strengths. We set the step position to be fixed before recombination era $1 + z_{c,1} = 2500$ and let the fraction of energy density f_1 varies for different cases.

Parameter	Best-fit Model 4	Best-fit Model 3	Best-fit Model 5
n_1	> 1.42	> 1.46	> 1.47
w_1	$0.787^{+0.064}_{-0.092}$	0.808 ± 0.060	$0.820^{+0.073}_{-0.032}$
Ω_m	0.2933 ± 0.0080	0.2838 ± 0.0085	$0.2703^{+0.0089}_{-0.0061}$
H_0	70.37 ± 0.68	$71.83^{+0.59}_{-0.67}$	$73.84^{+0.49}_{-0.92}$
S_8	0.873 ± 0.017	0.890 ± 0.018	$0.903^{+0.018}_{-0.014}$
$10^9 A_s$	2.058 ± 0.027	2.052 ± 0.029	2.053 ± 0.030
n_s	0.9815 ± 0.0042	0.9932 ± 0.0044	1.0098 ± 0.0055
τ	0.0449 ± 0.0060	0.0425 ± 0.0065	$0.0414^{+0.0063}_{-0.0077}$

Table 4. Observational constraints and %68 limits for parameters of **One-Step** models with different values for f_1 (cf. table 3) based on CMB+BAO+SN data. The higher is the value of f_1 , the larger is the prediction for H_0 .

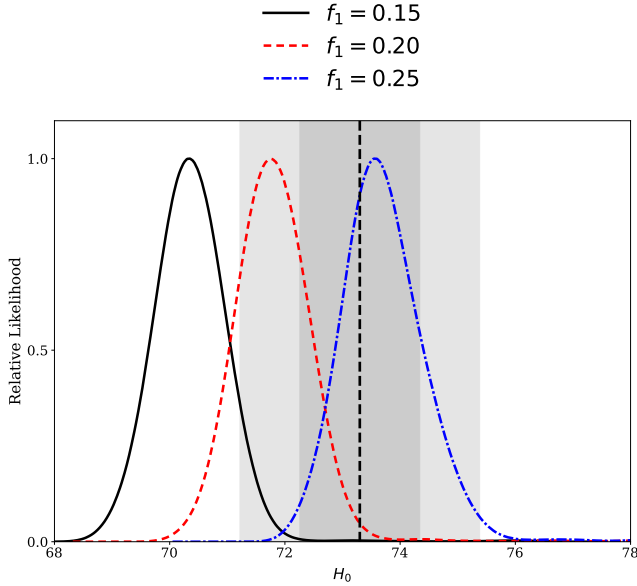


Figure 4. One-dimensional likelihoods for **One-Step** models with different values of f_1 for H_0 based on CMB+BAO+SN data. Note that the shaded area shows measurement of H_0 done by SH0ES team and its 1σ error (Riess et al. 2021).

2σ allowed error regions based on SH0ES measurements for H_0 (Riess et al. 2021).

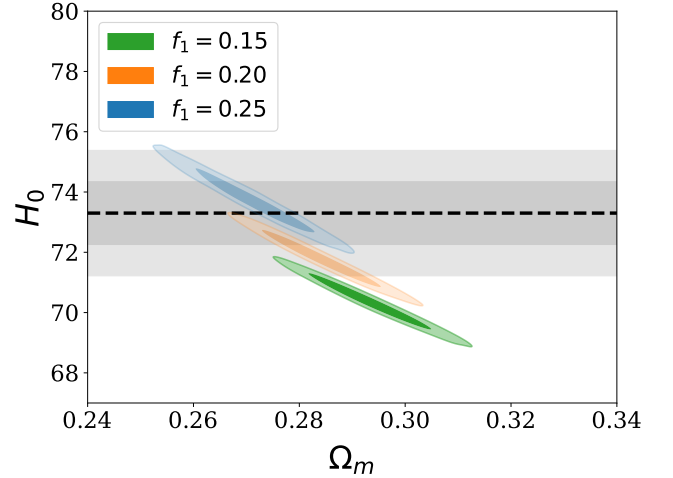


Figure 5. Contour plots for **One-Step** models with different values of f_1 for H_0 vs. Ω_m based on CMB+BAO+SN data. Note that the shaded area shows measurement of H_0 done by SH0ES team and its 1σ error (Riess et al. 2021).

4.2. Two-Step models

Here, we extend our analysis to some Two-Step class of models. In this type of models the first transition in dark energy can occur in more earlier time while the second transition can take place before the surface of last scattering or after that. Also, we have freedom in choosing the second phase of dark energy to be dS type or AdS type.

4.2.1. Effect of position of second step

In this approach we assume the first step is fixed at the time $1 + z_{c,1} = 2500$ and test different positions for the second step of evolution. In Table. 5 we present our assumptions for priors of parameters. Since we consider the first step to occur before the surface of last scattering, we assume the second step to occur after the surface of last scattering. In addition, in all of the models in this subsection we assume a dS phase for second step (positive values for f_2).

Looking at Table. 6 we see that the result for H_0 does not strongly depend on the position of the second step (as long as the sign of f_2 is fixed). For example in the the Models 6, 7 and 8, the values of $z_{2,c}$ change by two orders of magnitude while H_0 does not change drastically. Having said this, we notice that the value of H_0 in Model 6, where the second step occurs more closer to CMB era, shows more consistency with the SH0ES measurements. On the other hand, by putting the second step closer to late-time (Model 8) H_0 shows more tension.

In Figs. 6 and 7 we present the likelihoods and contour plots for H_0 and Ω_m in Two-Step models with different position of second step.

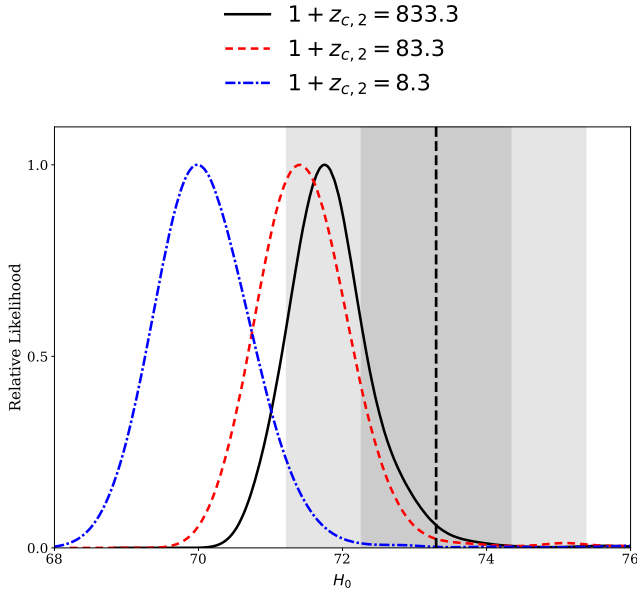


Figure 6. One-dimensional likelihoods for **Two-Step** models for H_0 based on CMB+BAO+SN data comparing the effect of second step position $z_{c,2}$ with fixed $f_1, f_2 > 0$.

4.2.2. Considering dS or AdS for second step

As mentioned above in Two-Step and Three-Step models we have the freedom in choosing the next phases to be dS-like or AdS-like. Hence, we want to test the effect of having a dS or an AdS in the second phase of evolution. In Table. 7

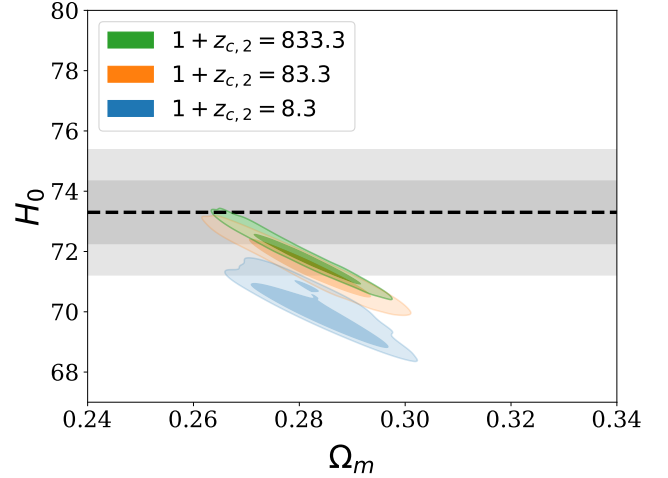


Figure 7. Contour plots for **Two-Step** models for H_0 vs. Ω_m based on CMB+BAO+SN data comparing the effect of the second step position $z_{c,2}$ with fixed $f_1, f_2 > 0$. Note that the shaded area shows measurement of H_0 done by SH0ES team and its 1σ error (Riess et al. 2021).

we have priors for two models: Model 7 and Model 9 that have similar priors but with opposite signs for f_2 .

In Table. 8 we summarize observational constrains for parameters of Model 7 and Model 9 while in Figs. 8 and 9 we see likelihoods and contour plots for H_0 and Ω_m in these two models. Clearly, having the second phase to be AdS-type, yields to a higher value of H_0 . Furthermore, in this numerical example the second phase to be AdS-type shows more consistency with the SH0ES measurements.

To confirm these conclusions, we have repeated this comparison for the Models 10 and 11 as well which have opposite signs of f_2 , with the priors given in Table. 9 while the results are summarized in Table. 10. In Figs. 10 and 11 we see likelihoods and contour plots for H_0 and Ω_m in these two models. As expected, a second phase in AdS-type yields to a higher value of H_0 .

4.3. Three-Step models

As a wider extension of our study we extend the analysis to the models with three steps of transitions in dark energy. As before, we assume the first phase is dS-type happening at early time at $z_{c,1} = 2500$ while the second and thirist steps can happen near or long after the surface of last scattering with either dS or AdS type. As described in Table. 11, we have tested different permutations of the signs of f_2 and f_3 parameters.

According to Table. 12 and Table. 13 different cases of three-step class of models show consistency with SH0ES results. However, as we see from table 13, Model 12 and Model 13 show the least tension with SH0ES measurements. In Model 12 all three steps are in dS phase but in Model 13 the second step is chosen to be AdS phase. The corresponding results are presented in Fig. 12 for the likelihood probabili-

Parameter	Priors	Priors	Priors
	Model 6	Model 7	Model 8
$1 + z_{c,1}$	2500	2500	2500
f_1	0.20	0.20	0.20
w_1	[0.5, 1]	[0.5, 1]	[0.5, 1]
n_1	[-1, 1.5]	[-1, 1.5]	[-1, 1.5]
$1 + z_{c,2}$	833	83.3	8.3
f_2	0.10	0.10	0.10
w_2	[0.5, 1]	[0.5, 1]	[0.5, 1]
n_2	[-1, 1.5]	[-1, 1.5]	[-1, 1.5]

Table 5. Priors for **Two-Step** models with different second step positions $1 + z_{c,2}$ while all other inputs are the same. We choose the first step to occur before recombination era $1 + z_{c,1} = 2500$ and let the second step to occur after recombination but in three different era.

Parameter	Best-fit	Best-fit	Best-fit
	Model 6	Model 7	Model 8
n_1	> 1.47	> 1.42	> 1.46
w_1	> 0.984	$0.763^{+0.036}_{-0.057}$	$0.703^{+0.033}_{-0.043}$
n_2	> 0.363	---	---
w_2	> 0.730	< 0.641	< 0.576
Ω_m	$0.2801^{+0.0081}_{-0.0055}$	$0.2811^{+0.0085}_{-0.0068}$	0.2832 ± 0.0076
H_0	$71.92^{+0.39}_{-0.74}$	$71.55^{+0.52}_{-0.77}$	$70.11^{+0.59}_{-0.76}$
S_8	$0.876^{+0.017}_{-0.013}$	0.875 ± 0.021	0.853 ± 0.017
$10^9 A_s$	2.019 ± 0.031	$2.039^{+0.025}_{-0.036}$	$2.017^{+0.026}_{-0.030}$
n_s	0.9843 ± 0.0048	$0.9989^{+0.0050}_{-0.0044}$	$1.0085^{+0.0052}_{-0.0044}$
τ	0.0426 ± 0.0072	$0.0434^{+0.0058}_{-0.0078}$	$0.0448^{+0.0056}_{-0.0063}$

Table 6. %68 limits for parameters of **Two-Step** models based on CMB+BAO+SN data. Note that all the input parameters are the same and only the position of the second step $z_{c,2}$ is different (cf. table 5). While $z_{c,2}$ changes by two orders of magnitude in these examples, but H_0 does not change significantly.

ties and also for contour plots of H_0 vs. Ω_m in Fig. 13. A general conclusion is that having the second and third phases both to be in AdS type, $f_2, f_3 < 0$, leads to higher values of H_0 compared to the cases where they are both in dS phases, $f_2, f_3 > 0$, compare Models 12 and 15. However, the competition is more non-trivial when a dS phase and an AdS phase are both present, i.e. the cases where $f_2 > 0, f_3 < 0$ compared to the case where $f_2 < 0, f_3 > 0$, see Models 13 and 14.

5. SUMMARY AND DISCUSSIONS

We studied a phenomenological model in which dark energy undergoes multiple transient stages. At early time prior to transition, the dark energy behaves like a small cosmological constant term. At the transition time, dark energy comprises a noticeable fraction of the total energy density and falls off rapidly afterwards. The equation of state of the fluid after transition is represented by the parameter w with the requirement $\frac{1}{3} < w \leq 1$ in order not to modify the expansion history of universe drastically. While this is a phenomenological proposal which can mimic EDE scenario, but it may be

realized theoretically as well. For example, this setup may be realized within the context of vacuum zero point energy of quantum fields in connection to the cosmological constant problem. Alternatively, this proposal may emerge from theories beyond SM of particle physics where the energy density of hidden sector do not interact with the SM fields while they contribute in the expansion history of the universe.

We have studied various cases of single transition, double transition and triple transition in dark energy density. In the latter two cases we also allowed that the second and/or third components of dark energy to be either dS-like ($\rho_x > 0$) or AdS-like ($\rho_x < 0$). As in standard EDE setup, having a larger value of f_1 yields to a larger value of H_0 . In addition, AdS-like dark energy yields to larger values of H_0 . To solve the H_0 tension, as in EDE scenario, the first transition is located sometime between the time of matter radiation equality and the surface of last scattering, say at the redshift $z_{c,1} \sim 2500$. However, the second or third transitions can take place anytime after the CMB decoupling. We have considered the cases where these happen say at redshifts $z_{c,2} \sim 800$ and $z_{c,3} \sim 80$. Our investigations show

Parameter	Priors	Priors
	Model 7	Model 9
$1 + z_{c,1}$	2500	2500
f_1	0.20	0.20
w_1	[0.5, 1]	[0.5, 1]
n_1	[-1, 1.5]	[-1, 1.5]
$1 + z_{c,2}$	83.3	83.3
f_2	+0.10	-0.10
w_2	[0.5, 1]	[0.5, 1]
n_2	[-1, 1.5]	[-1, 1.5]

Table 7. Priors for **Two-Step** models with different signs for f_2 . As in standard EDE scenario, we choose the first step to be a dS type $f_1 > 0$ while let the second step to be either dS type ($f_2 > 0$) or AdS type ($f_2 < 0$). Other parameters are the same.

Parameter	Best-fit	Best-fit
	Model 7	Model 9
n_1	> 1.42	> 1.46
w_1	$0.763^{+0.036}_{-0.057}$	0.827 ± 0.061
n_2	— — —	> 0.783
w_2	< 0.641	> 0.794
Ω_m	$0.2811^{+0.0085}_{-0.0068}$	$0.2832^{+0.0078}_{-0.0070}$
H_0	$71.55^{+0.52}_{-0.77}$	$72.19^{+0.54}_{-0.72}$
S_8	0.875 ± 0.021	$0.895^{+0.017}_{-0.015}$
$10^9 A_s$	$2.039^{+0.025}_{-0.036}$	2.060 ± 0.029
n_s	$0.9989^{+0.0050}_{-0.0044}$	0.9914 ± 0.0046
τ	$0.0434^{+0.0058}_{-0.0078}$	0.0427 ± 0.0065

Table 8. Best-fit values and %68 confidence intervals for parameters of **Two-Step** models based on CMB+BAO+SN data. Everything is similar in two cases but sign of f_2 is opposite (cf. table 7).

Parameter	Priors	Priors
	Model 10	Model 11
$1 + z_{c,1}$	2500	2500
f_1	0.25	0.25
w_1	[0.5, 1]	[0.5, 1]
n_1	[-1, 1.5]	[-1, 1.5]
$1 + z_{c,2}$	83.3	83.3
f_2	0.15	-0.15
w_2	[0.5, 1]	[0.5, 1]
n_2	[-1, 1.5]	[-1, 1.5]

Table 9. Priors for **Two-Step** models with opposite sign of f_2 . This is similar to Table 7 for Models 7 and 9 but here we have increased both f_1 and $|f_2|$ compared to Table 7.

that the resulting values of H_0 is not sensitive to the locations of the second or third transitions ($z_{c,2}$ and $z_{c,3}$) but it is largely sensitive to the value and the signs of the fraction of dark energy, f_2 and f_3 . Our analysis also shows that to obtain values of H_0 comparable to the value obtained from the local measurements requires that n_s to move towards the Harrison-Zeldovich scale invariant value. In all the examples

which we studied so far the least tension in H_0 value occurs in a Three-Step model in which all of its phases of evolution are dS-like ($f_i > 0, i = 1, 2, 3$).

As we mentioned previously, in the current analysis we have concentrated only on the background evolution as the physics behind the dark energy transition was already complicated at the background level. A fully consistent analysis

Parameter	Best-fit Model 10	Best-fit Model 11
n_1	> 1.46	> 1.41
w_1	0.762 ± 0.036	$0.824^{+0.087}_{-0.044}$
n_2	< 0.957	> 1.07
w_2	< 0.534	> 0.786
Ω_m	$0.2662^{+0.0078}_{-0.0061}$	$0.267^{+0.011}_{-0.0052}$
H_0	$73.18^{+0.48}_{-0.81}$	$74.70^{+0.34}_{-1.2}$
S_8	$0.875^{+0.017}_{-0.015}$	$0.904^{+0.025}_{-0.013}$
$10^9 A_s$	$2.021^{+0.026}_{-0.032}$	2.060 ± 0.031
n_s	$1.0223^{+0.0054}_{-0.0047}$	1.0077 ± 0.0069
τ	$0.0414^{+0.0059}_{-0.0067}$	$0.0420^{+0.0061}_{-0.0087}$

Table 10. Summary of observational constraints and %68 limits for parameters of **Two-Step** models based on CMB+BAO+SN data comparing effects of sign of f_2 , dS or AdS (cf. table 9, similar to table. 8 for Models 7 and 9).

Parameter	Priors Model 12	Priors Model 13	Priors Model 14	Priors Model 15
$1 + z_{c,1}$	2500	2500	2500	2500
f_1	0.25	0.25	0.25	0.25
w_1	[0.5, 1]	[0.5, 1]	[0.5, 1]	[0.5, 1]
n_1	[-1, 1.5]	[-1, 1.5]	[-1, 1.5]	[-1, 1.5]
$1 + z_{c,2}$	833	833	833	833
f_2	+0.15	-0.15	+0.15	-0.15
w_2	[0.5, 1]	[0.5, 1]	[0.5, 1]	[0.5, 1]
n_2	[-1, 1.5]	[-1, 1.5]	[-1, 1.5]	[-1, 1.5]
$1 + z_{c,3}$	83.3	83.3	83.3	83.3
f_3	+0.15	+0.15	-0.15	-0.15
w_3	[0.5, 1]	[0.5, 1]	[0.5, 1]	[0.5, 1]
n_3	[-1, 1.5]	[-1, 1.5]	[-1, 1.5]	[-1, 1.5]

Table 11. Priors for **Three-Step** models with different signs of the fractions of dark energy density f_2, f_3 in second and third steps. We fix the first step in dS phase $f_1 > 0$ and test different permutations of dS or AdS phases for second and third steps.

of the effects of transient dark energies requires the perturbations to be included as well. While this is beyond the scope of the current analysis but it is an interesting question to extend the current analysis where the perturbations are included as well.

We are grateful to Sunny Vagnozzi and E. Di Valentino for insightful comments and discussions. H. F. and A. T. would like to thank the “Saramadan” federation of Iran for the partial supports. H.F. would like to thank YITP, Kyoto University for the hospitality during the workshop “Gravity: Current challenge in black hole physics and cosmology” where this work was in progress.

REFERENCES

- Addison, G. E., Huang, Y., Watts, D. J., et al. 2016, *Astrophys. J.*, 818, 132
- Aghanim, N., et al. 2017, *Astron. Astrophys.*, 607, A95
- . 2020a, *Astron. Astrophys.*, 641, A5
- . 2020b, *Astron. Astrophys.*, 641, A6, [Erratum: *Astron. Astrophys.* 652, C4 (2021)]
- . 2020c, *Astron. Astrophys.*, 641, A8
- Agrawal, P., Cyr-Racine, F.-Y., Pinner, D., & Randall, L. 2019, arXiv:1904.01016
- Aiola, S., et al. 2020, *JCAP*, 12, 047
- Akarsu, O., Barrow, J. D., Escamilla, L. A., & Vazquez, J. A. 2020, *Phys. Rev. D*, 101, 063528
- Akarsu, O., Kumar, S., Özlüker, E., & Vazquez, J. A. 2021, *Phys. Rev. D*, 104, 123512

Parameter	Best-fit Model 12	Best-fit Model 13	Best-fit Model 14	Best-fit Model 15
n_1	> 1.46	> 1.46	> 1.46	> 1.46
w_1	> 0.991	$0.543^{+0.014}_{-0.025}$	> 0.994	$0.569^{+0.014}_{-0.026}$
n_2	> 0.600	> 1.07	> 1.06	> 1.14
w_2	> 0.905	> 0.865	$0.78^{+0.16}_{-0.11}$	> 0.940
n_3	— — —	< -0.762	> 0.682	> 0.992
w_3	< 0.530	< 0.521	> 0.865	> 0.873
Ω_m	$0.2634^{+0.0080}_{-0.0061}$	0.2586 ± 0.0073	$0.2641^{+0.0074}_{-0.0056}$	0.2585 ± 0.0076
H_0	$73.09^{+0.46}_{-0.83}$	74.08 ± 0.75	$74.60^{+0.42}_{-0.73}$	$75.70^{+0.56}_{-0.69}$
S_8	$0.861^{+0.019}_{-0.016}$	0.872 ± 0.019	$0.893^{+0.018}_{-0.015}$	$0.903^{+0.018}_{-0.016}$
$10^9 A_s$	$1.979^{+0.028}_{-0.031}$	2.022 ± 0.032	$2.013^{+0.025}_{-0.030}$	2.057 ± 0.028
n_s	1.0129 ± 0.0060	$1.0390^{+0.0053}_{-0.0039}$	$0.9979^{+0.0039}_{-0.0046}$	$1.0255^{+0.0044}_{-0.0039}$
τ	$0.0420^{+0.0059}_{-0.0069}$	0.0408 ± 0.0066	$0.0415^{+0.0057}_{-0.0066}$	0.0404 ± 0.0064

Table 12. Constraints of %68 limits and best-fit values for parameters of **Three-Step** models based on CMB+BAO+SN data (cf. table 11).

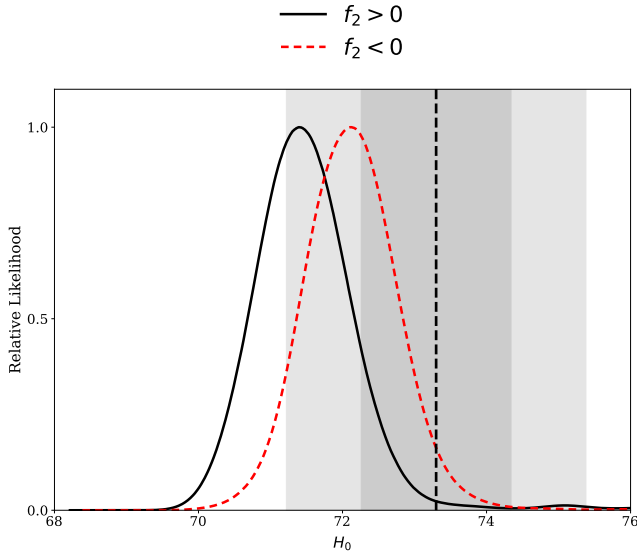


Figure 8. One-dimensional likelihoods for **Two-Step** models for H_0 based on CMB+BAO+SN data comparing the effect of the sign of f_2 , dS ($f_2 > 0$) or AdS ($f_2 < 0$) in Models 7 and 9.

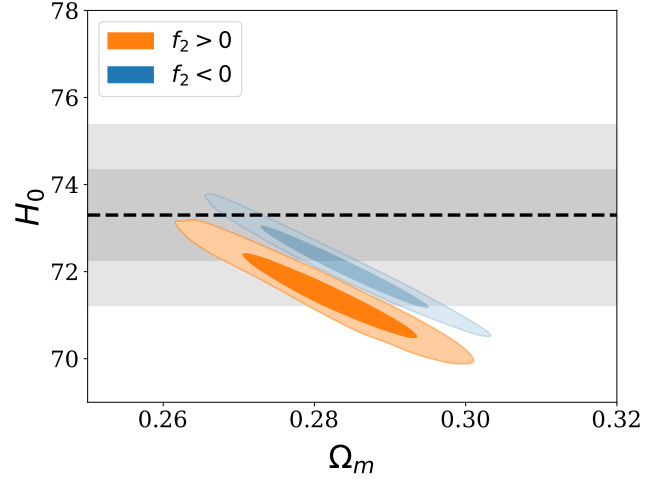


Figure 9. Contour plots for **Two-Step** models for H_0 vs. Ω_m based on CMB+BAO+SN data comparing the effect of the sign of f_2 , dS ($f_2 > 0$) or AdS ($f_2 < 0$) in Models 7 and 9. Note that the shaded area shows the measurement of H_0 done by SH0ES team and its 1σ error (Riess et al. 2021).

Alam, S., et al. 2017, Mon. Not. Roy. Astron. Soc., 470, 2617
Ballesteros, G., Notari, A., & Rompineve, F. 2020, JCAP, 11, 024
Banihashemi, A., Khosravi, N., & Shirazi, A. H. 2020, Phys. Rev. D, 101, 123521
Bernal, J. L., Verde, L., & Riess, A. G. 2016, JCAP, 10, 019
Beutler, F., Blake, C., Colless, M., et al. 2011, Mon. Not. Roy. Astron. Soc., 416, 3017
Braglia, M., Ballardini, M., Finelli, F., & Koyama, K. 2021, Phys. Rev. D, 103, 043528
Braglia, M., Emond, W. T., Finelli, F., Gumrukcuoglu, A. E., & Koyama, K. 2020, Phys. Rev. D, 102, 083513
Calderón, R., Gannouji, R., L’Huillier, B., & Polarski, D. 2021, Phys. Rev. D, 103, 023526

Chudaykin, A., Gorbunov, D., & Nedelko, N. 2020, JCAP, 08, 013
—, 2021, Phys. Rev. D, 103, 043529
Dainotti, M. G., De Simone, B., Schiavone, T., et al. 2021, Astrophys. J., 912, 150
—, 2022, Galaxies, 10, 24
D’Amico, G., Senatore, L., Zhang, P., & Zheng, H. 2021, JCAP, 05, 072
Di Valentino, E., & Bridle, S. 2018, Symmetry, 10, 585
Di Valentino, E., Melchiorri, A., Fantaye, Y., & Heavens, A. 2018, Phys. Rev. D, 98, 063508
Di Valentino, E., Melchiorri, A., & Silk, J. 2016, Phys. Lett. B, 761, 242
Di Valentino, E., Mena, O., Pan, S., et al. 2021a, Class. Quant. Grav., 38, 153001

Model	H_0	Gaussian Tension
Λ CDM	67.70 ± 0.52	5σ
One-Step cases (Tables: 1 & 3)		
Model 1	66.43 ± 0.54	7.9σ
Model 2	67.80 ± 0.52	3.87σ
Model 3	$71.83^{+0.59}_{-0.67}$	1.2σ
Model 4	70.37 ± 0.68	2.3σ
Model 5	$73.84^{+0.49}_{-0.92}$	0.47σ
Two-Step cases (Tables: 5 , 7 & 9)		
Model 6	$71.92^{+0.39}_{-0.74}$	2.46σ
Model 7	$71.55^{+0.52}_{-0.77}$	2.83σ
Model 8	$70.11^{+0.59}_{-0.76}$	2.66σ
Model 9	$72.19^{+0.54}_{-0.72}$	0.94σ
Model 10	$73.10^{+0.50}_{-0.73}$	0.17σ
Model 11	$74.70^{+0.34}_{-1.2}$	1.27σ
Three-Step cases (Table: 11)		
Model 12	$73.09^{+0.46}_{-0.83}$	0.07σ
Model 13	74.08 ± 0.75	0.58σ
Model 14	$74.60^{+0.42}_{-0.73}$	1.02σ
Model 15	$75.70^{+0.56}_{-0.69}$	1.76σ

Table 13. H_0 tension criteria for One-Step, Two-Step and Three-Step models in comparison to Λ CDM model.

- Di Valentino, E., et al. 2021b, *Astrophys. J.*, 131, 102605
- Dutcher, D., et al. 2021, *Phys. Rev. D*, 104, 022003
- Dutta, K., Ruchika, Roy, A., Sen, A. A., & Sheikh-Jabbari, M. M. 2020, *Gen. Rel. Grav.*, 52, 15
- Efstathiou, G. 2020, arXiv:2007.10716
- Farhang, M., & Khosravi, N. 2021, *Phys. Rev. D*, 103, 083523
- Firouzjahi, H. 2022a, arXiv:2205.06561
- . 2022b, arXiv:2201.02016
- Freedman, W. L., et al. 2019, arXiv:1907.05922
- Gelman, A., & Rubin, D. B. 1992, *Statist. Sci.*, 7, 457
- Gogoi, A., Sharma, R. K., Chanda, P., & Das, S. 2021, *Astrophys. J.*, 915, 132
- Gómez-Valent, A. 2022, arXiv:2203.16285
- Guo, R.-Y., Zhang, J.-F., & Zhang, X. 2019, *JCAP*, 02, 054
- Hagstotz, S., de Salas, P. F., Gariazzo, S., et al. 2021, *Phys. Rev. D*, 104, 123524
- Henning, J. W., et al. 2018, *Astrophys. J.*, 852, 97
- Herold, L., Ferreira, E. G. M., & Komatsu, E. 2022, *Astrophys. J. Lett.*, 929, L16
- Hill, J. C., McDonough, E., Toomey, M. W., & Alexander, S. 2020, *Phys. Rev. D*, 102, 043507
- Hill, J. C., et al. 2021, arXiv:2109.04451
- Ivanov, M. M., McDonough, E., Hill, J. C., et al. 2020, *Phys. Rev. D*, 102, 103502
- Jiang, J.-Q., & Piao, Y.-S. 2021, *Phys. Rev. D*, 104, 103524
- . 2022, *Phys. Rev. D*, 105, 103514
- Kaloper, N. 2019, *Int. J. Mod. Phys. D*, 28, 1944017
- Karwal, T., & Kamionkowski, M. 2016, *Phys. Rev. D*, 94, 103523

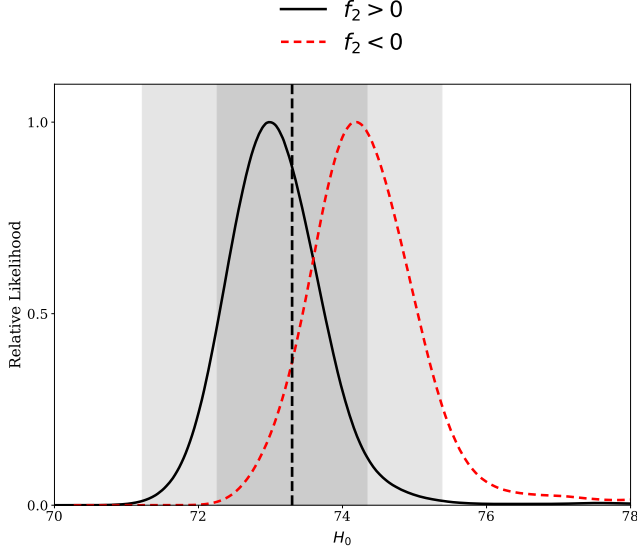


Figure 10. One-dimensional likelihoods for **Two-Step** models for H_0 based on CMB+BAO+SN data, comparing the effects of the sign of f_2 in Models 10 and 11. This plot is parallel to Fig. 8 performed for Models 7 and 9 but now the value of f_1 is increased to $f_1 = 0.25$ and the values of f_2 in dS and AdS cases are changed to $f_2 = +0.15$ and $f_2 = -0.15$ respectively.

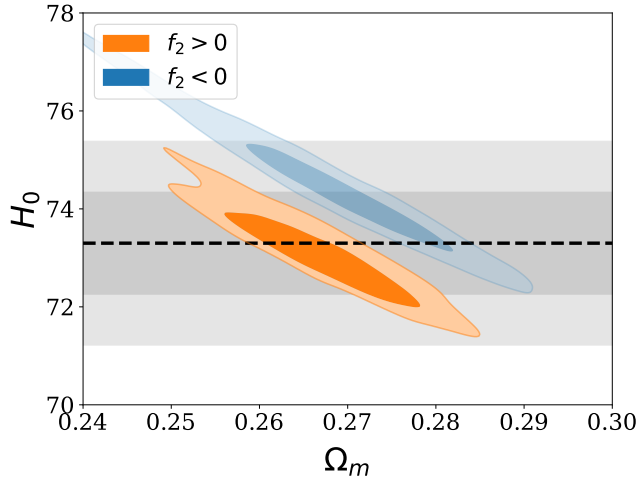


Figure 11. Contour plots for **Two-Step** models for H_0 vs. Ω_m based on CMB+BAO+SN data comparing the effects of sign of f_2 . The rest of the description is as in Fig. 10.

- Karwal, T., Raveri, M., Jain, B., Khoury, J., & Trodden, M. 2022, Phys. Rev. D, 105, 063535
- Khosravi, N., & Farhang, M. 2022, Phys. Rev. D, 105, 063505
- Knox, L., & Millea, M. 2020, Phys. Rev. D, 101, 043533
- Krishnan, C., Colgáin, E. O., Ruchika, et al. 2020, Phys. Rev. D, 102, 103525
- La Posta, A., Louis, T., Garrido, X., & Hill, J. C. 2021, arXiv:2112.10754

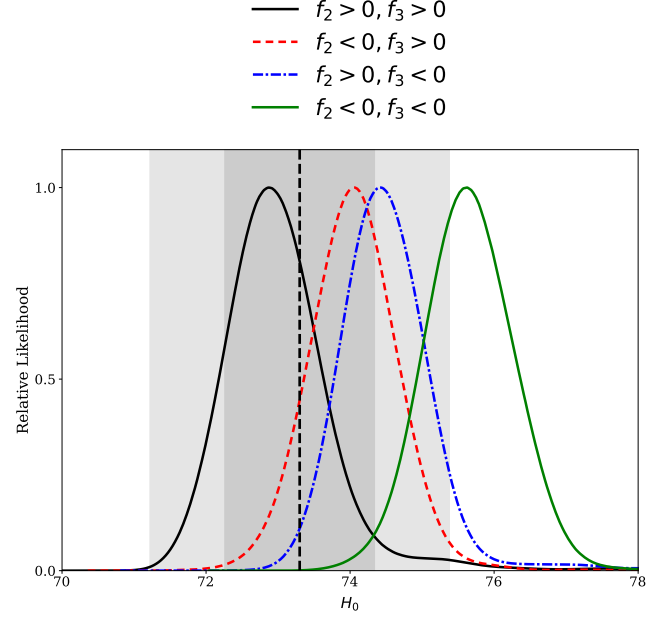


Figure 12. One-dimensional likelihoods for **Three-Step** models for H_0 based on “CMB+BAO+SN” data comparing the effects of the signs of the fraction of dark energy in the second and third phases (f_2, f_3) with a fixed $f_1 > 0$.

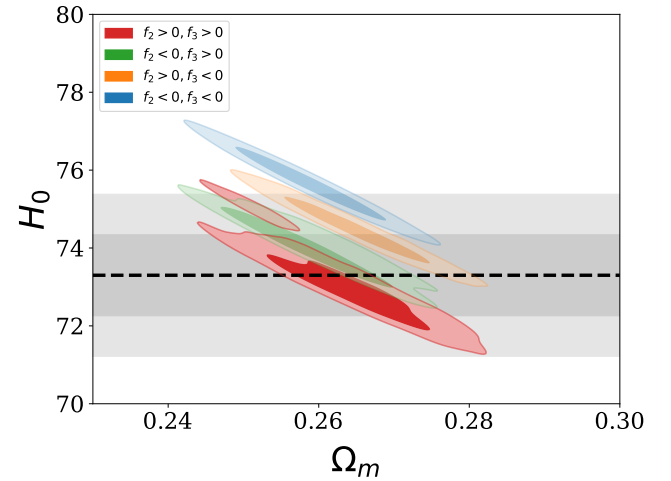


Figure 13. Contour plots for **Three-Step** models for H_0 vs. Ω_m based on “CMB+BAO+SN” data comparing the effects of the signs of the fraction of dark energy in the second and third phases (f_2, f_3) with a fixed $f_1 > 0$. Note that the shaded area shows measurement of H_0 done by SH0ES team and its 1σ error (Riess et al. 2021).

- Lemos, P., Lee, E., Efstathiou, G., & Gratton, S. 2019, Mon. Not. Roy. Astron. Soc., 483, 4803
- Lewis, A. 2013, Phys. Rev. D, 87, 103529
- Lewis, A., & Bridle, S. 2002, Phys. Rev. D, 66, 103511
- Lin, M.-X., Benevento, G., Hu, W., & Raveri, M. 2019, Phys. Rev. D, 100, 063542
- Lin, M.-X., Hu, W., & Raveri, M. 2020, Phys. Rev. D, 102, 123523

- Martin, J. 2012, *Comptes Rendus Physique*, 13, 566
- Mörtsell, E., & Dhawan, S. 2018, *JCAP*, 09, 025
- Mortsell, E., Goobar, A., Johansson, J., & Dhawan, S. 2021, arXiv:2105.11461
- Moshafi, H., Baghran, S., & Khosravi, N. 2021, *Phys. Rev. D*, 104, 063506
- Motloch, P., & Hu, W. 2020, *Phys. Rev. D*, 101, 083515
- Murgia, R., Abellán, G. F., & Poulin, V. 2021, *Phys. Rev. D*, 103, 063502
- Niedermann, F., & Sloth, M. S. 2021, *Phys. Rev. D*, 103, L041303
- Nojiri, S., Odintsov, S. D., Saez-Chillon Gomez, D., & Sharov, G. S. 2021, *Phys. Dark Univ.*, 32, 100837
- Nunes, R. C., & Vagnozzi, S. 2021, *Mon. Not. Roy. Astron. Soc.*, 505, 5427
- Perivolaropoulos, L., & Skara, F. 2021, arXiv:2105.05208
- Poulin, V., Smith, T. L., & Bartlett, A. 2021, *Phys. Rev. D*, 104, 123550
- Poulin, V., Smith, T. L., Karwal, T., & Kamionkowski, M. 2019, *Phys. Rev. Lett.*, 122, 221301
- Reeves, A., Herold, L., Vagnozzi, S., Sherwin, B. D., & Ferreira, E. G. M. 2022, arXiv:2207.01501
- Riess, A. G. 2019, *Nature Rev. Phys.*, 2, 10
- Riess, A. G., et al. 2021, arXiv:2112.04510
- Ross, A. J., Samushia, L., Howlett, C., et al. 2015, *Mon. Not. Roy. Astron. Soc.*, 449, 835
- Ruchika, Adil, S. A., Dutta, K., Mukherjee, A., & Sen, A. A. 2020, arXiv:2005.08813
- Sakstein, J., & Trodden, M. 2020, *Phys. Rev. Lett.*, 124, 161301
- Schöneberg, N., Franco Abellán, G., Pérez Sánchez, A., et al. 2021, arXiv:2107.10291
- Scolnic, D. M., et al. 2018, *Astrophys. J.*, 859, 101
- Sen, A. A., Adil, S. A., & Sen, S. 2021, arXiv:2112.10641
- Seto, O., & Toda, Y. 2021, *Phys. Rev. D*, 103, 123501
- Smith, T. L., Lucca, M., Poulin, V., et al. 2022, arXiv:2202.09379
- Smith, T. L., Poulin, V., & Amin, M. A. 2020, *Phys. Rev. D*, 101, 063523
- Smith, T. L., Poulin, V., Bernal, J. L., et al. 2021, *Phys. Rev. D*, 103, 123542
- Vagnozzi, S. 2020, *Phys. Rev. D*, 102, 023518
- Verde, L., Treu, T., & Riess, A. G. 2019, *Nature Astron.*, 3, 891
- Visinelli, L., Vagnozzi, S., & Danielsson, U. 2019, *Symmetry*, 11, 1035
- Ye, G., Hu, B., & Piao, Y.-S. 2021a, *Phys. Rev. D*, 104, 063510
- Ye, G., & Piao, Y.-S. 2020a, *Phys. Rev. D*, 101, 083507
- , 2020b, *Phys. Rev. D*, 102, 083523
- Ye, G., Zhang, J., & Piao, Y.-S. 2021b, arXiv:2107.13391
- Zumalacarregui, M. 2020, *Phys. Rev. D*, 102, 023523